METEOROLOGICAL APPLICATIONS
Meteorol. Appl. (2014)
Published online in Wiley Online Library
(wileyonlinelibrary.com) DOI: 10.1002/met.1451

Inter-comparison of radar-based nowcasting schemes in the Jianghuai River Basin, China

Gaili Wang,[a,b] Yang Hong,[b]* Liping Liu,[a] Wai Kin Wong,[c] Ali Zahraei[d] and Valliappa Lakshmanan[e]

[a] *State Key Laboratory of Severe Weather, Chinese Academy of Meteorological Science, Beijing, China*
[b] *School of Civil Engineering and Environmental Sciences and Advanced Radar Research Centre, University of Oklahoma, Norman, OK, USA*
[c] *Hong Kong Observatory, China*
[d] *NOAA/CREST–Cooperative Remote Sensing Science and Technology Centre, City College of the City University of New York, NY, USA*
[e] *Cooperative Institute of Mesoscale Meteorological Studies, University of Oklahoma, and NOAA/National Severe Storms Laboratory, Norman, OK, USA*

ABSTRACT: The primary objective of this study is to compare the forecasting skill of two nowcasting schemes, the Multi-scale Tracking Radar Echoes by Cross-correlation (MTREC) in current usage and the newly developed Multi-scale Tracking and Forecasting Radar Echoes (MTaFRE) used by the State Key Laboratory of Severe Weather (LaSW) of the Chinese Academy of Meteorological Science (CAMS), with the Eulerian Persistence Model (EPM) scheme as a benchmark, and the state-of-the-art Watershed-Clustering Nowcasting (WCN) scheme, which is part of the Warning Decision Support System-Integrated Information (WDSS-II) developed at the University of Oklahoma and the National Severe Storms Laboratory (NSSL). The inter-comparison considers six heavy-rain events and one month of radar data observed by radar networks of the Chinese Meteorological Administration (CMA) located in the Jianghuai River Basin. Four sets of forecast fields up to the next 180 min with an interval of 15 min were generated by the four nowcasting algorithms, and the forecast performances were evaluated as a function of lead time. At an individual event level, the results show that no single model outperforms all others consistently in cross-skill categories at all lead-time intervals of the six events. Overall, EPM performs worse than the three Lagrangian persistent models (LPMs). The MTREC scheme performs slightly worse than the WCN scheme used in WDSS-II, and the MTaFRE scheme is most comparable to the WCN scheme. More importantly, this study confirms that the MTaFRE shows an improvement over its predecessor MTREC by using multi-scale moving mean windows effectively for different lead times.

KEY WORDS inter-comparison; nowcasting; forecast performances; radar mosaic

Received 29 September 2013; Revised 5 December 2013; Accepted 6 January 2014

1. Introduction

Heavy rain is one of the most severe weather systems in China's Jianghuai River Basin, and causes severe flooding and geological disasters such as landslides. High-resolution quantitative nowcasting (0–3 h) can play an important role in effectively improving disaster early warning system for emergency response and management. In general, two main methods including storm-scale numerical weather prediction (NWP) models and extrapolation techniques are used for nowcasting (Ganguly and Bras, 2003; Zahraei *et al.*, 2012). With the recent development of high-performance computer systems and data assimilation techniques, storm-scale NWP models with atmospheric dynamic constraints have been used to enhance short-term forecasting. For example, an NWP model with suitable data assimilation can improve short-term precipitation forecasting significantly by assimilating radar data (Macpherson, 2001; Weygandt *et al.*, 2002; Caya *et al.*, 2005; Tong and Xue, 2005; Sokol, 2007). However, because the data are sensitive to the initial field, NWP forecasting skill may not be regarded as optimal for very short-term predictions (Golding, 1998; Benjamin *et al.*, 2004). Moreover, a high-resolution NWP model running in a horizontal grid spacing of a few kilometres used in conjunction with the data assimilation process requires powerful computers to provide forecasts in real time (Sokol and Pesice, 2012). Therefore, extrapolation techniques based on radar data, which have lower computational demands, are still applied often to very short-term forecasts of precipitation.

A number of techniques for short-term forecasting of severe weather have been developed in the past several decades for extrapolating the observed radar patterns to the next 0–3 h. These nowcasting techniques can be classified broadly into object-based and pixel-based approaches. The object-based technique has the ability to identify storms as objects and to track and forecast storm-related characteristic parameters such as areas, mass centroids and maximum reflectivity (Dixon and Wiener, 1993; Johnson *et al.*, 1998, Hong *et al.*, 2004; Vila *et al.*, 2008; Zahraei *et al.*, 2013). The pixel-based technique considers radar echo movement between two consecutive radar patterns, and extrapolates observations in the pixel scale (Rinehart and Garvey, 1978; Li *et al.*, 1995; Grecu and Krajewski, 2000; Germann and Zawadzki, 2002, 2004; Zahraei *et al.*, 2012). For example, a commonly used robust technique

* Correspondence: Y. Hong, School of Civil Engineering and Environmental Sciences and Advanced Radar Research Centre, University of Oklahoma, 120 David L. Boren Blvd., National Weather Centre Rm. 4610, Norman, Oklahoma, USA. E-mail: yanghong@ou.edu

for estimating echo movement *via* the correlation method is known as Tracking Radar Echoes by Correlation (TREC; Rinehart and Garvey, 1978; Tuttle and Foote, 1990; Tuttle and Gall, 1999). Comparisons have been performed among different nowcasting models, and the results generally indicate that even complex models such as the neural-network, which considers complex storm dynamic Lagrangian evolution, are similar to relatively simple advection schemes (Grecu and Krajewski, 2000; Montanari *et al.*, 2006).

Several very short-term quantitative nowcasting techniques based on the correlation method have been applied extensively in China. To eliminate the chaotic vectors of the TREC vectors caused by rapid changes of echoes, the Difference Image-based Tracking Radar Echo by Correlations (DITREC) method was introduced. However, this method results in some pixels less than the threshold to be ignored (Zhang *et al.*, 2006). To extend the extrapolation algorithm for forecasting up to 3 h ahead, a blending approach that combines TREC vectors with model-predicted winds has also been studied (Liang *et al.*, 2009). In view of storm motion being considered as a combination of macro-scale steering level winds and micro-scale storm internal motion (Germann *et al.*, 2006), the Multi-scale Tracking Radar Echoes by Cross-correlation (MTREC) technique was proposed to retrieve simultaneously multi-scale echo motion in order to eliminate the zero vectors effectively (Wang *et al.*, 2013).The present study aims to assess the latest development of nowcasting schemes used by the Chinese Academy of Meteorological Science (CAMS) through inter-comparison of their forecast performances with other baseline or state-of-the-art nowcasting models in the Jianghuai River Basin. These models include (1) the Eulerian Persistence Model (EPM) scheme as a baseline, (2) the Watershed-Clustering Nowcasting (WCN) scheme embedded in the Warning Decision Support System–Integrated Information (WDSS–II; Lakshmanan *et al.*, 2007a) developed by the National Severe Storm Laboratory (NSSL) and the University of Oklahoma (Lakshmanan *et al.*, 2003, 2009), (3) the MTREC scheme currently used by CAMS, and (4) the newly developed Multi-scale Tracking and Forecasting Radar Echoes (MTaFRE) scheme.

The paper is organised as follows. A short overview of the study domain and datasets and a brief description of the four nowcasting schemes including EPM, WCN, MTREC, and MTaFRE are given in Sections 2 and 3, respectively. The performance indices are listed in Section 4, and the evaluation results based on six heavy rain events and 1 month of radar data are presented in Section 5. The conclusions and discussions are presented in Section 6.

2. Datasets

Six heavy rainfall events and 1 month of radar data during August 2009 were considered in this study. Figure 1 gives the study domain, in which eight S-band radar positions are marked with triangles. Radar data were measured by the Chinese Meteorological Administration (CMA) radar network at 6 min intervals. With its limited detection range, a single radar is insufficient for covering widespread rain or large-scale precipitation systems. The composite radar reflectivity mosaics generated by the Doppler Weather Radar 3D Digital Mosaic System (RDMS), which was developed by the State Key Laboratory of Severe Weather (LaSW) of CAMS, were used in this study to track and nowcast reflectivity fields (Wang *et al.*, 2009). The major steps of RDMS include quality control for

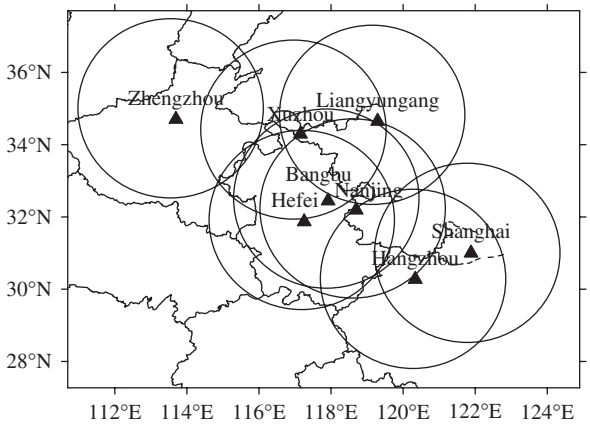

Figure 1. The study domain and locations (as triangles) of Doppler radars.

single radar, interpolation from spherical co-ordinates onto a Cartesian grid, and a 3D mosaic. The single radar reflectivity data underwent quality control to remove non-precipitation targets, including ground clutter, electronic interference and anomalous propagations. The reflectivity data were then interpolated from spherical co-ordinates onto a 3D Cartesian grid *via* nearest neighbour on range-azimuth planes combined with a linear interpolation in a vertical direction scheme. Once the reflectivity data of all radars were interpolated to the Cartesian co-ordinates, interpolated reflectivity values at any given grid in the Cartesian co-ordinates were combined *via* an exponential weighting average scheme to yield the final mosaic reflectivity value at the grid point (Zhang *et al.*, 2004; Xiao and Liu, 2006). RDMS produces two types of products at a high temporal resolution of 6 min and a spatial resolution of 0.01 °. The first type is 3D reflectivity mosaics including a maximum of 40 levels with adjustable vertical resolution and a default resolution of 500 m at low levels, and the second is 2D composite radar reflectivity mosaics obtained by processing the 3D data. The 2D composite radar reflectivity mosaics rather than rainfall rate patterns were used in this study for nowcasting and assessment. The reason is that rainfall rate is liable to be affected by source errors such as inappropriate radar reflectivity–rainfall rate (Z–R) relationships, hail and bright band contamination (Wilson and Brandes, 1979; Zawadzki, 1984; Lakshmanan *et. al*, 2007b; Xu *et al.*, 2008; Lakshmanan *et al.*, 2010; Wang *et al.*, 2012; Qi *et al.*, 2013).

Climatologically, heavy floods often occur in summer and autumn in China, during which heavy rainfall events are usually prolonged and intense. To compare the forecasting skill among the four nowcasting schemes, six heavy rain events and 1 month of radar data during the rainy season were selected. Figure 2 shows one representative image of each event, and Table 1 lists several characteristics of the selected six events on the basis of statistical characteristics of precipitation events reported by Germann and Zawadzki (2002). The first event observed on 7 June 2009 was quite extended and dominated relatively by stratiform clouds. The second event occurred on 19 June 2009, and included a considerable convective fraction and was relatively loose. The third event represents a coherent and large storm that occurred on 16 August 2009, which was dominated by convective activities. The fourth event is a coherent, relatively small, and slow-moving convection system (stationary storm). In the fifth and sixth events, convective cells produced precipitation predominantly, where the rain area was

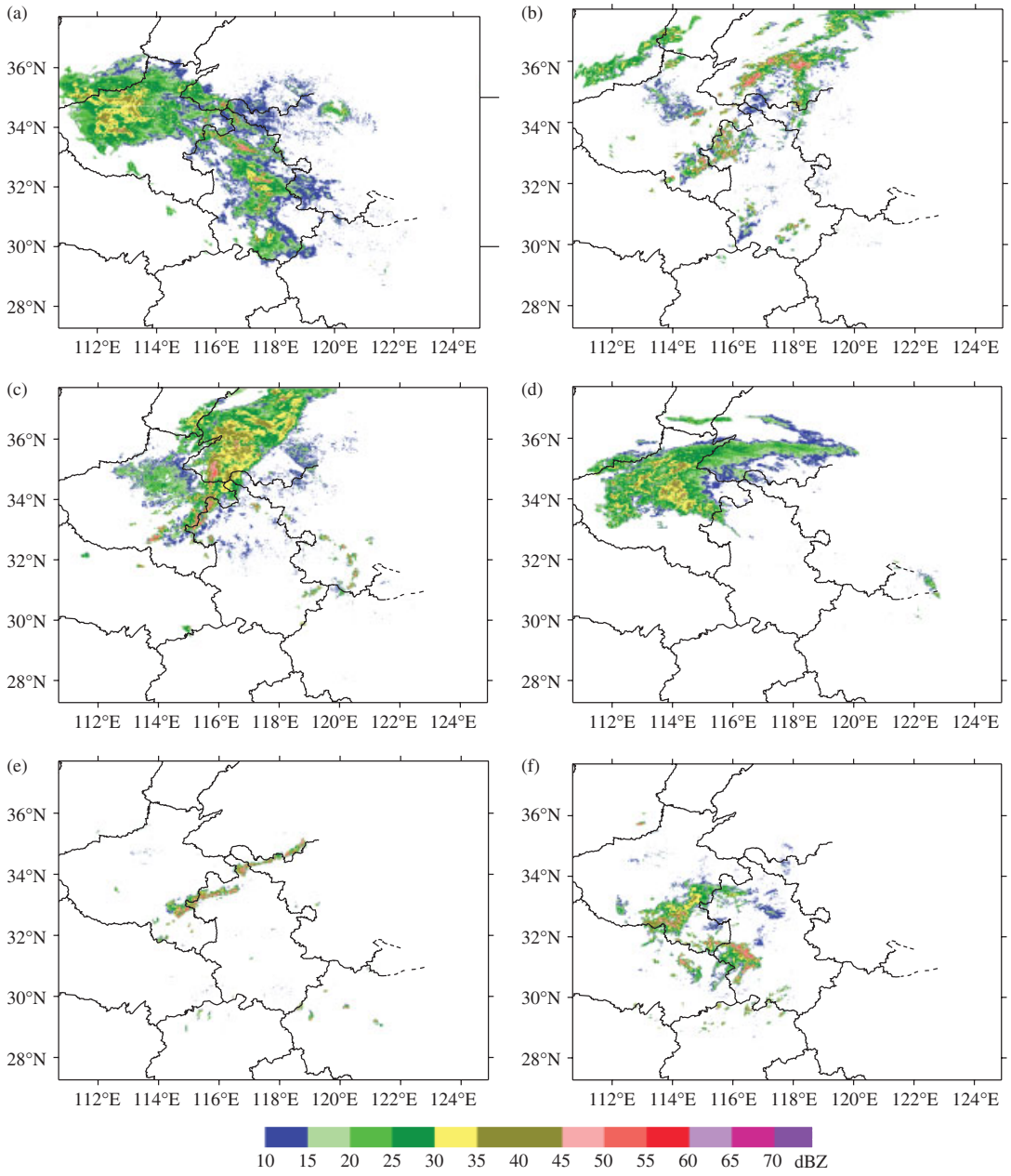

Figure 2. Mosaic images for four heavy rain events used in this study. Image at 1500 UTC on 7 June 2009 for event 1 (a), image at 0800 UTC on 19 June 2009 for event 2 (b), image at 0800 UTC on 17 August 2009 for event 3 (c), and image at 0400 UTC 24 September 2009 for event 4 (d), image at 0700 UTC on 26 August 2009 for event 5 (e), and image at 0500 UTC on 28 August 2009 for event 6 (f).

Table 1. Statistics of the four precipitation events used in this study.

Event	Date	Start (UTC)	Duration (h)	Raining area (10^4 km^2)	>25 dBZ (%)	>40 dBZ (%)
1	7–8 June 2009	0300	46	18	34	3
2	19 June 2009	0200	18	6	44	7
3	16–17 August 2009	0600	40	10	42	5
4	24 September 2009	0000	23	11	34	2
5	26 August 2009	0500	9	3	45	13
6	28 August 2009	0100	10	5	39	8

relatively small and the lifetime of precipitation pattern was relatively short.

3. Nowcasting models

This study aims to assess the performance of MTREC and its enhanced scheme MTaFRE nowcasting techniques based on radar patterns developed by CAMS. The inter-comparison was performed among four different nowcasting models. The other two models used were EPM and WCN. The EPM scheme was selected for its ease of application and was treated as a baseline. The WCN scheme used in WDSS–II was selected for its state-of-the-art level of nowcasting skill. The four different nowcasting models forecast reflectivity fields up to the next 180 min with intervals of 15 min. The reflectivity threshold for tracking and forecasting was set to 10 dBZ, which corresponds to a precipitation rate of 0.1 mm h^{-1}. Reflectivity lower than the threshold was considered as no rain because the minimum

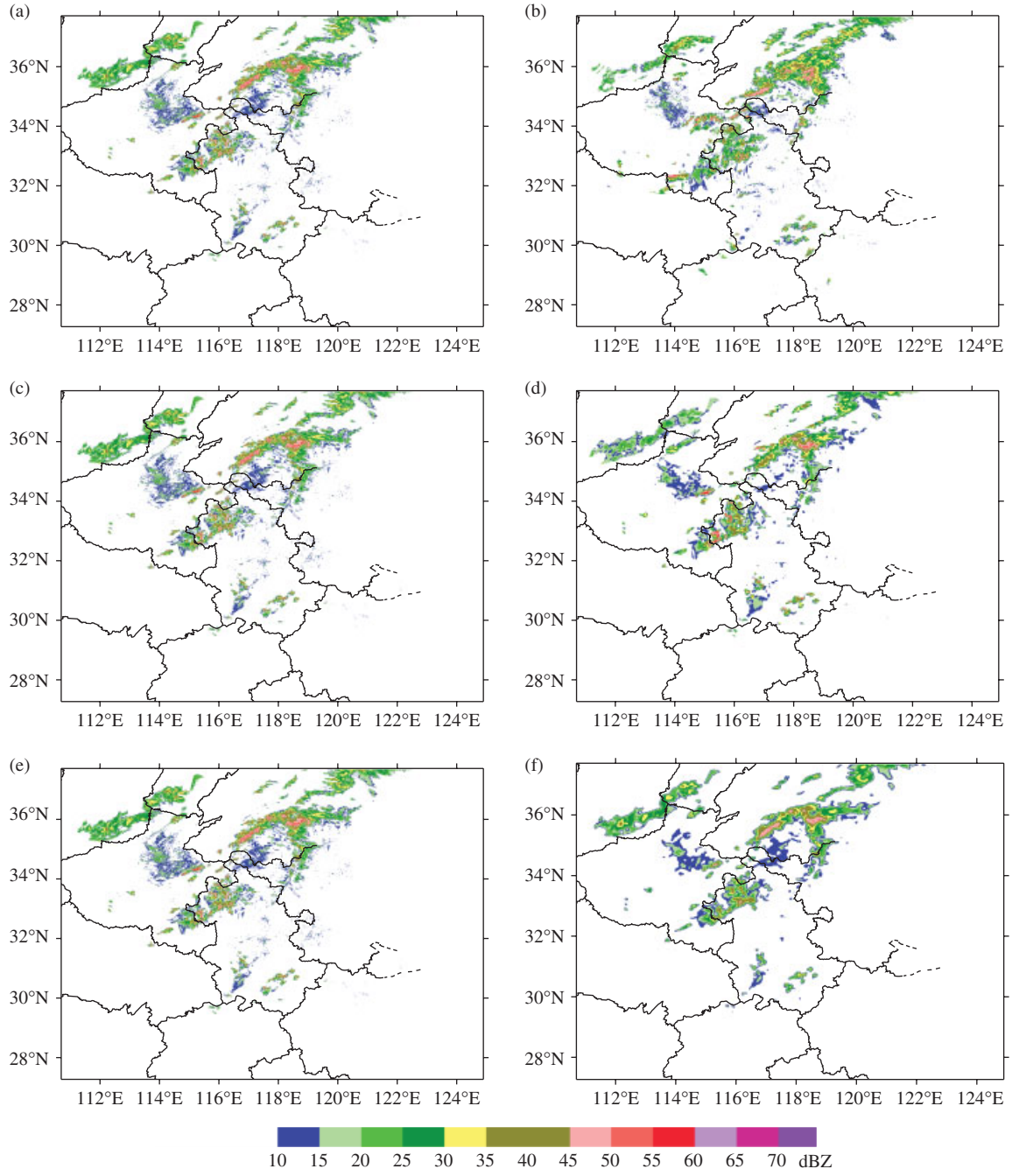

Figure 3. Event 2 on 19 June 2009, 0800 (base time) and 0900 UTC observation (a, b), EPM + 60[min] prediction and WCN + 60[min] prediction (c, d), MTREC + 60[min] prediction and MTaFRE + 60[min] prediction (e, f).

rainfall amount required for tilting the tipping bucket rain gauge is 0.1 mm in China.

3.1. Eulerian-Persistence Model (EPM)

The EPM assumes that precipitation remains stationary. That is, the future precipitation image is equivalent to the last available image (Montanari *et al.*, 2006). This situation can be expressed as:

$$\frac{\Delta F_t\,(x,y)}{\Delta t} = 0 \qquad (1)$$

where $F_t(x,y)$ is radar reflectivity at pixel (x, y), and $\Delta F_t(x,y)$ denotes reflectivity variation at pixel (x, y). The EPM is simple and applied easily. Therefore, the EPM was considered as a baseline for assessing the performances of complex nowcasting models.

3.2. Watershed-Clustering Nowcasting (WCN)

The WCN scheme works operationally in the WDSS–II system developed by NSSL and the University of Oklahoma. This scheme is an object-based approach that includes identification, tracking and extrapolation of storms. Clustering is used to identify storms, with a minimization cost function considering both intensity and position of each pixel. The cost function is

Table 2. Performance indices with error bar for the lead time of 60 min. Bold values indicate the best performance among the four considered nowcasting models.

	Scheme	Event 1	Event 2	Event 3	Event 4	Event 5	Event 6
d	EPM	0.56 ± 0.005	0.46 ± 0.012	0.63 ± 0.004	0.65 ± 0.001	0.32 ± 0.013	0.43 ± 0.005
	WCN	0.61 ± 0.007	0.53 ± 0.012	0.67 ± 0.002	0.66 ± 0.002	0.40 ± 0.010	0.57 ± 0.004
	MTREC	0.57 ± 0.006	0.51 ± 0.014	0.65 ± 0.002	0.63 ± 0.003	0.39 ± 0.011	0.56 ± 0.003
	MTaFRE	0.61 ± 0.005	0.53 ± 0.014	0.69 ± 0.003	0.65 ± 0.002	0.41 ± 0.012	0.57 ± 0.004
CSI (threshold = 10 dBZ)	EPM	0.55 ± 0.007	0.38 ± 0.000	0.53 ± 0.007	0.62 ± 0.003	0.16 ± 0.003	0.35 ± 0.001
	WCN	$\mathbf{0.58} \pm 0.008$	$\mathbf{0.45} \pm 0.001$	0.56 ± 0.006	0.62 ± 0.000	0.25 ± 0.001	0.42 ± 0.003
	MTREC	0.56 ± 0.006	0.43 ± 0.003	0.54 ± 0.007	0.61 ± 0.005	0.24 ± 0.002	0.42 ± 0.002
	MTaFRE	0.57 ± 0.006	$\mathbf{0.45} \pm 0.001$	$\mathbf{0.58} \pm 0.007$	$\mathbf{0.63} \pm 0.001$	$\mathbf{0.26} \pm 0.002$	$\mathbf{0.44} \pm 0.000$
CSI (threshold = 25 dBZ)	EPM	0.28 ± 0.009	0.24 ± 0.009	0.42 ± 0.003	0.41 ± 0.006	0.05 ± 0.005	0.25 ± 0.009
	WCN	$\mathbf{0.38} \pm 0.008$	0.33 ± 0.012	0.47 ± 0.002	$\mathbf{0.43} \pm 0.003$	$\mathbf{0.11} \pm 0.006$	$\mathbf{0.35} \pm 0.007$
	MTREC	0.35 ± 0.008	0.34 ± 0.010	0.46 ± 0.003	0.41 ± 0.004	0.10 ± 0.003	0.33 ± 0.006
	MTaFRE	$\mathbf{0.38} \pm 0.006$	$\mathbf{0.35} \pm 0.015$	$\mathbf{0.50} \pm 0.003$	0.42 ± 0.003	$\mathbf{0.11} \pm 0.004$	$\mathbf{0.35} \pm 0.005$
RMSE (dBZ)	EPM	12.31 ± 0.032	18.11 ± 0.207	12.83 ± 0.134	10.78 ± 0.057	22.00 ± 0.208	18.80 ± 0.022
	WCN	11.32 ± 0.016	16.16 ± 0.178	12.03 ± 0.087	$\mathbf{10.53} \pm 0.133$	19.09 ± 0.116	15.02 ± 0.020
	MTREC	12.19 ± 0.025	16.45 ± 0.232	12.55 ± 0.094	11.31 ± 0.097	19.30 ± 0.152	15.18 ± 0.024
	MTaFRE	$\mathbf{11.24} \pm 0.023$	$\mathbf{15.79} \pm 0.216$	$\mathbf{11.57} \pm 0.097$	10.67 ± 0.113	$\mathbf{18.47} \pm 0.146$	$\mathbf{14.88} \pm 0.021$

defined by Lakshmanan and Smith (2009) as:

$$E(k) = \lambda d_m(k) + (1-\lambda) d_c(k) \qquad 0 \le \lambda \le 1 \qquad (2)$$

where $d_m(k)$ is defined as the intensity difference between the pixel intensity and the mean intensity of the k^{th} cluster, and $d_c(k)$ denotes the number of neighbouring pixels not belonging to the k^{th} cluster. Here λ indicates the weighting co-efficient and was set to 0.6 for all radar patterns (Lakshmanan *et al.*, 2003).

The algorithm identifies storms with a watershed transform model, in which a storm is defined on the basis of a size threshold. Multi-scale storms are identified by using multiple size thresholds, which were set to 100 and 400 km^2 in this study according to the literature reported by Lakshmanan and Smith (2010).

The cost function optimisation method is used to track storms in the WCN algorithm. The cost function is defined by combining the size and peak intensities of storms (Lakshmanan and Smith, 2010). For nowcasting purposes, the motion vectors are obtained by interpolating movement between storms, with successive patterns corrected by using a cost function based on mean absolute error (Lakshmanan *et al.*, 2003). The WCN method changes future echoes' intensity with linear evolution based on historical radar patterns.

The WCN approach was used in this study as that implemented in WDSS−II (Lakshmanan *et al.*, 2007a) with default settings. No attempt was made to tone the WCN settings to Chinese data characteristics.

3.3. Multi-scale Tracking Radar Echoes by Cross-correlation (MTREC)

The MTREC scheme is a pixel-based approach that uses a Lagrangian Persistent Model (LPM). The forecast formulation can be written as:

$$\frac{\Delta F_t(x,y)}{\Delta t} + U_x(x,y)\frac{\Delta F_t(x,y)}{\Delta x} + U_y(x,y)\frac{\Delta F_t(x,y)}{\Delta y} = 0 \qquad (3)$$

where $U_x(x,y)$ and $U_y(x,y)$ are the components of storm motion vector at pixel (x, y). According to the LPM, the forecast field at time $t + \Delta t$ is obtained from the following relationship:

$$\widehat{F}_{t+\Delta t}(x,y) = F_t(x - \Delta x, y - \Delta y) \qquad (4)$$

$\widehat{F}_{t+\Delta t}(x,y)$ was obtained from $F_t(x,y)$ by advection; Δx and Δy are displacement components at the lead time of Δt, respectively.

Estimation of storm motion in the MTREC scheme is based on multi-scale tracking radar echoes by cross-correlation using two consecutive composite radar reflectivity mosaics.

The directions in which echoes move at different scales are not always consistent (Houze *et al.*, 1993). Storm motion is also considered as a combination of macro-scale steering level winds and micro-scale storm internal motion (Germann *et al.*, 2006). Furthermore, zero vectors, small vectors and vectors with directions opposite to those of their surrounding vectors, are the main sources that cause chaotic vectors. For these reasons, the MTREC scheme was introduced (Wang *et al.*, 2013) to improve the retrieval of storm motion at various horizontal scales.

The MTREC scheme estimates the storm motion vector through the following main steps:

(i) determine the macro-scale steering level winds by using the TREC technique with large boxes;
(ii) advect the reflectivity field from time t_0 to t_1;
(iii) on the basis of the extrapolated radar reflectivity field from step (ii) and that at time t_1, compute internal micro-scale motion vectors by using the TREC technique with small boxes;
(iv) synthesize the motion fields from steps (i) and (iii) and apply a smoothing procedure to generate the final gridded motion vectors.

By synthesising macro-scale steering level winds and storm internal micro-scale motion, MTREC vectors eliminate zero vectors and create more continuous motion vectors. The default sizes of the large and small boxes were set to $3^\circ \times 3^\circ$ and $0.2^\circ \times 0.2^\circ$, respectively (Wang *et al.*, 2013). Once the storm motion vectors are retrieved, the current radar pattern is advected up to the target lead time, which is 3 h in the present study.

The semi-Lagrangian advection scheme, characterized by rotation, mass conservation, and accurate calculation, is used

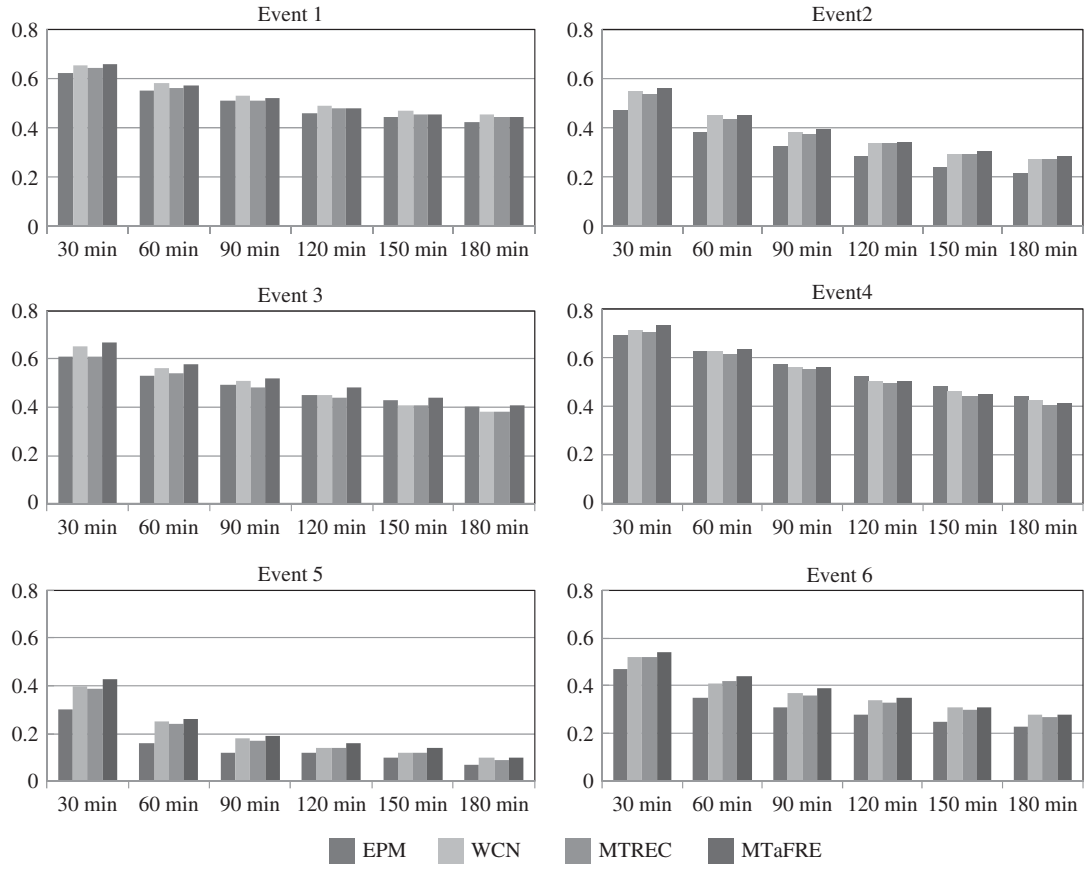

Figure 4. Critical success index with lead time for threshold of 10 dBZ.

widely to advect radar reflectivity (Germann and Zawadzki, 2002; Pradeep *et al.*, 2012). This scheme divides the lead time of Δt into N steps to advect, for each time step, displacements Δx_i and Δy_i, which are determined iteratively as:

$$\Delta x_i = (\Delta t/N)\, U_x\,(x - \Delta x_{i-1}, y - \Delta y_{i-1}) \tag{5}$$

$$\Delta y_i = (\Delta t/N)\, U_y\,(x - \Delta x_{i-1}, y - \Delta y_{i-1}) \tag{6}$$

where i is equal to $1, 2, \ldots, N$.

It is known that to obtain the velocity and value of the departure point in the semi-Lagrangian scheme, interpolation of neighbourhood grid point values is required. A mass-conserving, monotonic advection scheme based on the explicit remapped particle-mesh semi-Lagrangian (RPMSL) (Reich, 2007) advection scheme was used to extrapolate reflectivity in this study, ignoring growth and dissipation of precipitation. The length step was chosen to be 15 min. The explicit RPM SL advection scheme blends a low-order basis function by using bilinear splines and a high-order approximation with bicubic B-splines to implement interpolation.

3.4. Multi-Scale Tracking and Forecasting Radar Echoes (MTaFRE)

In this scheme, precipitation patterns are characterised with multi-scale information: small-scale precipitation features are perishable and less predictable; and the range of predictability increases with increasing scale (Bellon and Zawadzki, 1994; Germann and Zawadzki, 2002; Seed, 2003; Turner *et al.*, 2004). Optimum smoothing as a function of lead time is performed to improve forecast accuracy. The optimal smoothing window length is given by:

$$L = kT^{\lambda} \tag{7}$$

where L is the moving average window in km, T denotes lead time in minutes, and k, λ are empirical co-efficients with ranges of $1.0 \le k \le 1.3$ and $0.7 \le \lambda \le 0.8$, respectively. The relationship depends only on the assessment parameter and is independent of precipitation classification (Bellon and Zawadzki, 1994; Seed, 2003).

To improve forecast accuracy, moving average as a function of lead time is also applied to the MTREC scheme to perform multi-scale forecasting, and the enhanced scheme is called Multi-scale Tracking and Forecasting Radar Echoes (MTaFRE). For the degree of smoothing not related to characteristics of precipitation, in this study both k and λ were set to 0.8, the value was the same as that used by Bellon and Zawadzki (1994). In view of the step length of 15 min and iterative characteristics of the semi-Lagrangian advection scheme, a moving average with a window of 7×7 pixels (approximately $7 \times 7\,\mathrm{km}^2$) was applied iteratively to each output based on Equation (7).

The RPMSL advection scheme was also used to extrapolate reflectivity in the MTaFRE scheme, ignoring growth and dissipation of precipitation.

4. Performance indices

The following four performance indices were used to assess the skill of each of the considered nowcasting schemes: correlation

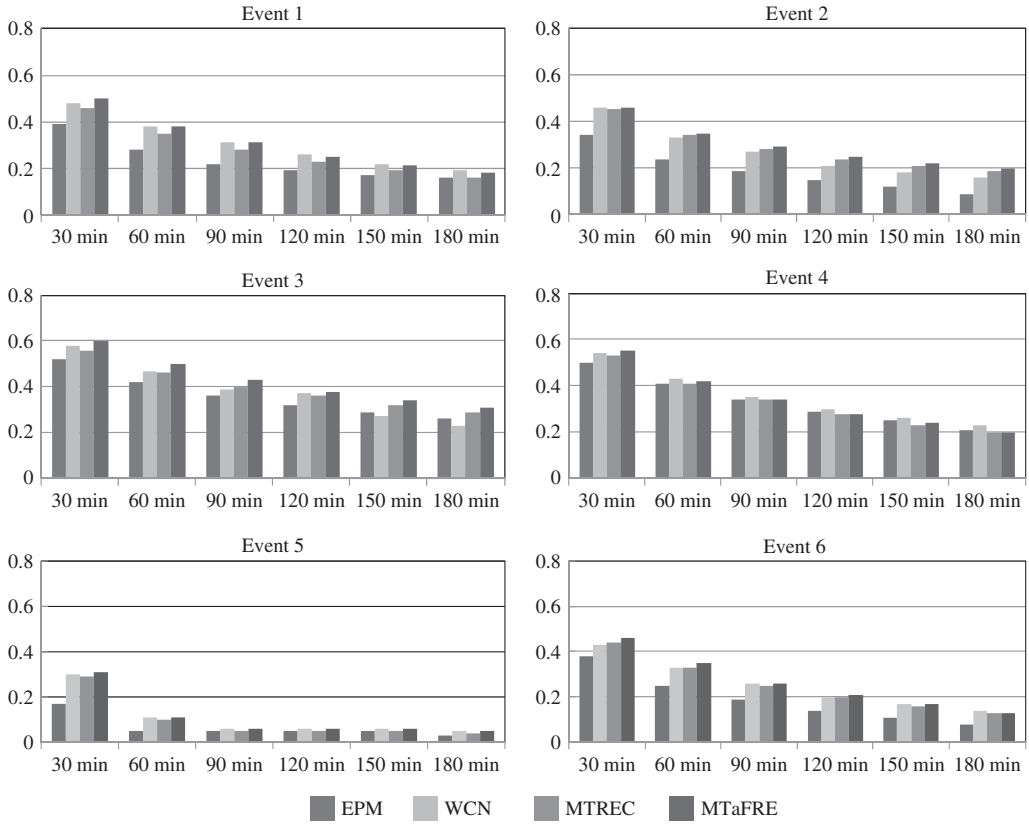

Figure 5. Critical success index with lead time for threshold of 25 dBZ.

co-efficient (CC), index of agreement (d), critical success index (CSI), and root mean square error (RMSE).

CC can be computed by:

$$\mathrm{CC} = \frac{\sum_{i=1}^{N} \left(O_i - \overline{O}\right)\left(F_i - \overline{F}\right)}{\sqrt{\sum_{i=1}^{N} \left(O_i - \overline{O}\right)^2 \sum_{i=1}^{N} \left(F_i - \overline{F}\right)^2}} \tag{8}$$

where O_i and F_i are the observed and predicted reflectivity at the i^{th} grid point, respectively, and the bar indicates the mean value. The range of the correlation co-efficient varies from 0 to 1.0, and values equal to 1.0 are perfect predictions. However, the correlation co-efficient has the disadvantage of not being sensitive to linear differences of observation and prediction (Legates and McCabe, 1999).

To cover the shortage, the index of agreement d was defined to measure the agreement between the observation and the forecast (Legates and McCabe, 1999):

$$d = 1 - \frac{\sum_{i=1}^{N} (O_i - F_i)^2}{\sum_{i=1}^{N} (|O_i - \overline{O}| + |F_i - \overline{O}|)^2} \tag{9}$$

The range of index of agreement is from 0 to 1.0, and values equal to 1.0 indicate perfect predictions.

To quantify the pattern match of observation and forecast, forecasting skills such as probability of detection (POD), false alarm ratio (FAR), and CSI are calculated. Because CSI could reflect the forecasting skill by integrating POD and FAR, CSI was selected for pattern match metrics. CSI is defined as:

$$\mathrm{CSI} = \frac{n_s}{n_s + n_f + n_a} \tag{10}$$

where n_s, n_f and n_a are the number of successes, failures and false alarms, respectively. The concepts of these parameters are the same as those depicted in several other studies (Grecu and Krajewski, 2000; Zahraei *et al.*, 2012). CSI will be between 0 and 1.0, and the values of 1.0 denote perfect predictions. In this study, two reflectivity thresholds of 10 and 25 dBZ were selected to calculate the CSI. These two thresholds correspond to precipitation rates of 0.1 and 1.0 mm h^{-1}, respectively.

Germann and Zawadzki (2002) stated that neither the correlation co-efficient nor the forecasting skill provided a direct measure of forecast accuracy. Thus, RMSE is calculated as:

$$\mathrm{RMSE} = \sqrt{\frac{\sum_{i=1}^{N} (F_i - O_i)^2}{N}} \tag{11}$$

RMSE ranges from 0 to ∞, and the smaller values correspond to better predictions.

5. Results and discussion

The six events listed in Table 1 and 1 month of radar data during August 2009 were examined for inter-comparison of the forecast performances among the four nowcasting models on the

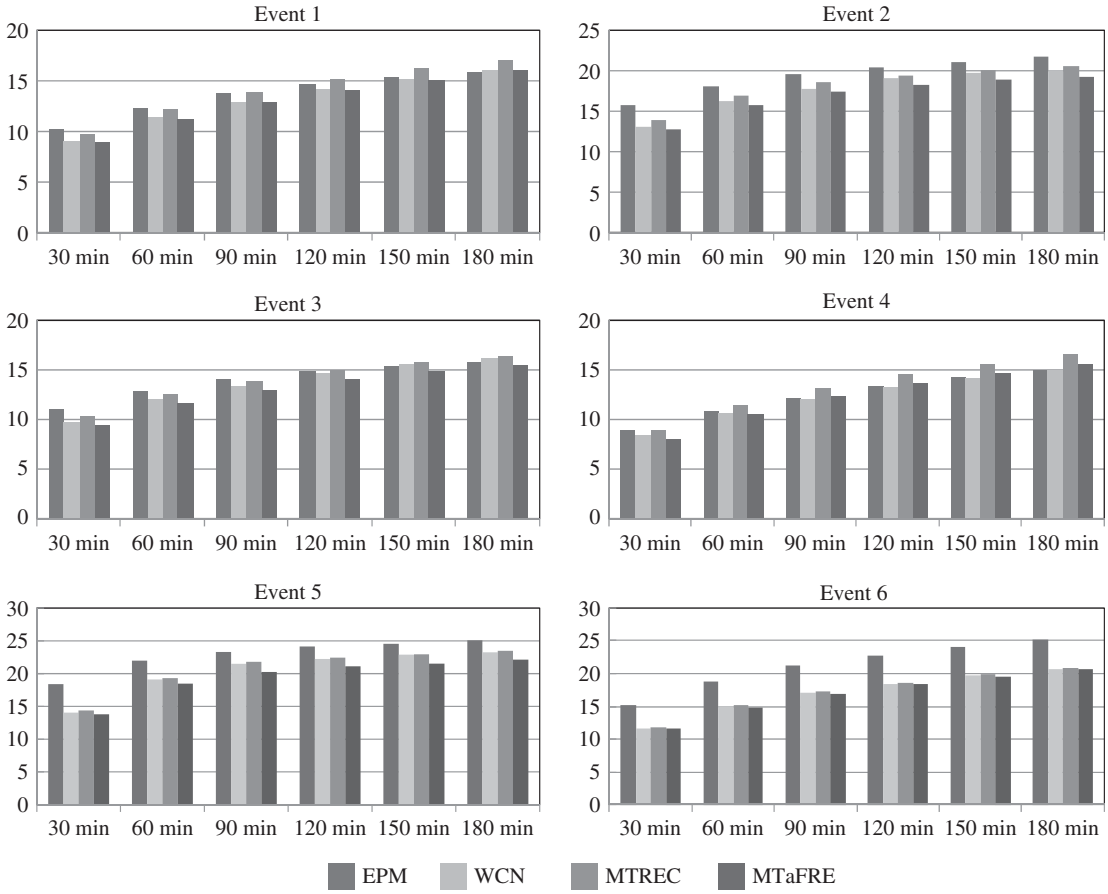

Figure 6. Root mean square error with lead time.

basis of radar mosaic patterns. For each radar mosaic pattern, four sets of forecast schemes up to the next 180 min with intervals of 15 min were generated by the EPM, WCN, MTREC, and MTaFRE models with a spatial resolution of $0.01^\circ \times 0.01^\circ$. The corresponding observed mosaic patterns with the same spatial resolution were used to verify the nowcasting outputs. For observed mosaic patterns with intervals of 6 min, the performance indices were calculated at intervals of 30 min. Because the first 30 min forecasts all appear to be satisfactory among the four models, except for relatively small and rapidly moving storm event 5, the forecasted results at a lead time of 60 min are discussed first, followed by those at a maximum of 180 min.

Considering that the extrapolation technique could not forecast the storm initialisation, the forecast performances were evaluated over the period from storm initialisation to disappearance for the considered six events.

5.1. 60 min lead time

Figure 3 shows the forecasts of the four models at 60 min lead time at a base time of 0800 UTC on 19 June 2009, and corresponding observations. In general, all appeared similar to the observations. In addition, a position error of storms existed in the forecasts obtained from the EPM method, which assumes that the forecast is equal to the last available radar pattern. However, the storms moved mainly toward the east at a relatively fast speed of approximately 35 km h^{-1} for this event. On the contrary, the WCN approach estimates storm motions on the basis of successive radar patterns; the storm position forecast matched well with the observed radar patterns. Although the WCN model considers storm evolution based on historical radar patterns rather than those of steady state, intensity difference existed between predicted patterns and observations, particularly in the southeastern echoes. Tsonis and Austin (1981) have demonstrated that extrapolation of intensity and area shows little improvement in short-term predictions. Development of extrapolation techniques that forecast precisely the changing precipitation intensities over time remain a challenge. The MTREC model retrieves storm motion by cross-correlation based on two successive radar patterns, resulting in positions of forecast echoes consistent with observation. This scheme advects reflectivity by using a semi-Lagrangian scheme, ignoring growth and dissipation of precipitation. In addition, intensity difference existed between predicted patterns and observations. Moreover, the MTaFRE forecast is smoother than that of MTREC because local high-frequency components characterised by lower persistence are filtered out by using a moving average window iteratively, along with increasing lead time.

Table 2 summarises the quantitative forecast performances of the four models at 60 min lead time. EPM performed more poorly than the other three LPMs, which is in accordance with the findings reported by other studies (Grecu and Krajewski, 2000; Germann and Zawadzki, 2002; Turner *et al.*, 2004; Montanari *et al.*, 2006; Zahraei *et al.*, 2012). The MTREC scheme performed worse than the WCN scheme at the lead time of 60 min, as indicated by nearly all of the verification indices. The MTaFRE scheme was most comparable to the

Table 3. Correlation co-efficient with error bar for different lead times. Bold values indicate the best performance among the four considered nowcasting models.

Event	Scheme	30 min	60 min	90 min	120 min	150 min	180 min
1	EPM	0.45 ± 0.007	0.27 ± 0.012	0.18 ± 0.013	0.11 ± 0.014	0.08 ± 0.016	**0.07** ± 0.012
	WCN	0.54 ± 0.007	0.37 ± 0.015	**0.27** ± 0.016	0.18 ± 0.010	**0.12** ± 0.007	**0.07** ± 0.002
	MTREC	0.50 ± 0.009	0.35 ± 0.011	0.24 ± 0.013	0.13 ± 0.008	0.07 ± 0.003	0.03 ± 0.002
	MTaFRE	**0.55** ± 0.007	**0.38** ± 0.009	**0.27** ± 0.012	**0.19** ± 0.006	**0.12** ± 0.003	**0.07** ± 0.000
2	EPM	0.20 ± 0.023	0.07 ± 0.021	0.02 ± 0.018	−0.02 ± 0.003	−0.04 ± 0.001	−0.07 ± 0.000
	WCN	**0.40** ± 0.015	**0.22** ± 0.020	**0.15** ± 0.024	0.09 ± 0.019	0.07 ± 0.004	0.06 ± 0.003
	MTREC	0.36 ± 0.019	0.18 ± 0.024	0.12 ± 0.027	0.08 ± 0.012	0.06 ± 0.001	0.05 ± 0.009
	MTaFRE	**0.40** ± 0.018	0.21 ± 0.023	0.14 ± 0.025	**0.10** ± 0.012	**0.09** ± 0.002	**0.07** ± 0.010
3	EPM	0.52 ± 0.007	0.38 ± 0.007	0.30 ± 0.009	0.25 ± 0.008	0.21 ± 0.002	0.18 ± 0.005
	WCN	0.61 ± 0.007	0.45 ± 0.003	0.36 ± 0.006	0.28 ± 0.007	0.23 ± 0.005	0.19 ± 0.009
	MTREC	0.58 ± 0.006	0.42 ± 0.003	0.34 ± 0.005	0.28 ± 0.008	0.23 ± 0.006	0.19 ± 0.010
	MTaFRE	**0.62** ± 0.006	**0.48** ± 0.004	**0.39** ± 0.007	**0.33** ± 0.009	**0.28** ± 0.008	**0.23** ± 0.011
4	EPM	0.58 ± 0.003	0.43 ± 0.003	0.32 ± 0.006	0.23 ± 0.003	0.16 ± 0.010	0.11 ± 0.014
	WCN	0.61 ± 0.001	**0.46** ± 0.002	**0.34** ± 0.005	**0.27** ± 0.001	**0.21** ± 0.005	**0.16** ± 0.011
	MTREC	0.59 ± 0.001	0.40 ± 0.005	0.26 ± 0.003	0.16 ± 0.000	0.09 ± 0.005	0.04 ± 0.010
	MTaFRE	**0.63** ± 0.002	0.44 ± 0.002	0.29 ± 0.008	0.19 ± 0.006	0.11 ± 0.008	0.06 ± 0.012
	EPM	0.13 ± 0.024	0.02 ± 0.020	−0.01 ± 0.013	−0.05 ± 0.003	−0.10 ± 0.003	−0.14 ± 0.002
5	WCN	**0.33** ± 0.014	**0.19** ± 0.022	**0.13** ± 0.018	0.06 ± 0.012	**0.04** ± 0.006	**0.03** ± 0.004
	MTREC	0.30 ± 0.018	0.15 ± 0.020	0.10 ± 0.023	0.05 ± 0.009	0.03 ± 0.005	0.02 ± 0.007
	MTaFRE	**0.33** ± 0.015	0.18 ± 0.019	**0.13** ± 0.021	**0.07** ± 0.010	**0.04** ± 0.004	**0.03** ± 0.009
	EPM	0.18 ± 0.022	0.06 ± 0.018	0.01 ± 0.021	−0.03 ± 0.017	−0.05 ± 0.008	−0.09 ± 0.005
6	WCN	0.37 ± 0.015	**0.20** ± 0.014	**0.13** ± 0.024	0.09 ± 0.019	0.07 ± 0.012	**0.05** ± 0.004
	MTREC	0.35 ± 0.018	0.17 ± 0.016	0.11 ± 0.019	0.08 ± 0.015	0.06 ± 0.010	0.04 ± 0.006
	MTaFRE	**0.38** ± 0.016	0.19 ± 0.015	**0.13** ± 0.020	**0.10** ± 0.018	**0.08** ± 0.009	**0.05** ± 0.007

Table 4. Index of agreement with error bar for different lead times. Bold values indicate the best performance among the four considered nowcasting models.

Event	Scheme	30 min	60 min	90 min	120 min	150 min	180 min
1	EPM	0.66 ± 0.004	0.56 ± 0.005	0.50 ± 0.006	0.47 ± 0.004	0.45 ± 0.005	**0.44** ± 0.003
	WCN	**0.72** ± 0.004	**0.61** ± 0.007	**0.55** ± 0.007	**0.50** ± 0.002	**0.46** ± 0.001	0.43 ± 0.001
	MTREC	0.69 ± 0.004	0.57 ± 0.006	0.51 ± 0.005	0.46 ± 0.001	0.43 ± 0.002	0.40 ± 0.002
	MTaFRE	**0.72** ± 0.004	**0.61** ± 0.005	**0.55** ± 0.005	**0.50** ± 0.001	**0.46** ± 0.001	0.43 ± 0.003
2	EPM	0.53 ± 0.012	0.46 ± 0.012	0.43 ± 0.008	0.41 ± 0.001	0.39 ± 0.000	0.38 ± 0.000
	WCN	**0.64** ± 0.009	**0.53** ± 0.012	**0.49** ± 0.011	0.46 ± 0.010	0.44 ± 0.002	0.43 ± 0.001
	MTREC	0.62 ± 0.010	0.51 ± 0.014	0.47 ± 0.013	0.45 ± 0.005	0.44 ± 0.001	0.43 ± 0.004
	MTaFRE	**0.64** ± 0.010	**0.53** ± 0.014	**0.49** ± 0.013	**0.47** ± 0.005	**0.46** ± 0.001	**0.45** ± 0.005
3	EPM	0.71 ± 0.006	0.63 ± 0.004	0.59 ± 0.003	0.56 ± 0.003	0.54 ± 0.001	0.52 ± 0.001
	WCN	0.77 ± 0.006	0.67 ± 0.002	0.62 ± 0.003	0.56 ± 0.003	0.54 ± 0.003	0.52 ± 0.004
	MTREC	0.75 ± 0.005	0.65 ± 0.002	0.60 ± 0.002	0.57 ± 0.004	0.54 ± 0.004	0.52 ± 0.004
	MTaFRE	**0.78** ± 0.005	**0.69** ± 0.003	**0.63** ± 0.002	**0.60** ± 0.005	**0.57** ± 0.004	**0.55** ± 0.004
4	EPM	0.74 ± 0.002	0.65 ± 0.001	0.58 ± 0.005	0.53 ± 0.004	0.49 ± 0.002	0.46 ± 0.006
	WCN	**0.77** ± 0.002	**0.66** ± 0.002	**0.59** ± 0.001	**0.54** ± 0.001	**0.51** ± 0.002	**0.48** ± 0.007
	MTREC	0.75 ± 0.002	0.63 ± 0.003	0.55 ± 0.000	0.49 ± 0.003	0.45 ± 0.001	0.42 ± 0.003
	MTaFRE	**0.77** ± 0.002	0.65 ± 0.002	0.57 ± 0.003	0.51 ± 0.001	0.47 ± 0.003	0.44 ± 0.007
	EPM	0.48 ± 0.018	0.32 ± 0.013	0.28 ± 0.011	0.23 ± 0.009	0.20 ± 0.005	0.15 ± 0.001
5	WCN	0.58 ± 0.012	0.40 ± 0.010	0.37 ± 0.008	0.35 ± 0.006	**0.32** ± 0.003	**0.28** ± 0.000
	MTREC	0.56 ± 0.013	0.39 ± 0.011	0.35 ± 0.012	0.33 ± 0.008	0.30 ± 0.003	0.27 ± 0.003
	MTaFRE	**0.59** ± 0.010	**0.41** ± 0.012	**0.38** ± 0.010	**0.36** ± 0.007	**0.32** ± 0.002	**0.28** ± 0.001
	EPM	0.55 ± 0.010	0.43 ± 0.005	0.39 ± 0.011	0.37 ± 0.007	0.35 ± 0.002	0.33 ± 0.005
6	WCN	0.65 ± 0.008	**0.57** ± 0.004	**0.53** ± 0.008	0.50 ± 0.005	0.48 ± 0.000	**0.45** ± 0.003
	MTREC	0.63 ± 0.010	0.56 ± 0.003	0.51 ± 0.010	0.49 ± 0.007	0.47 ± 0.001	0.43 ± 0.001
	MTaFRE	**0.66** ± 0.009	**0.57** ± 0.004	**0.53** ± 0.012	**0.51** ± 0.005	**0.49** ± 0.002	**0.45** ± 0.002

WCN one and was slightly better in terms of the average CSI and RMSE in the six events. The results show clearly that the MTaFRE scheme improved the forecast accuracy over its predecessor, the MTREC. This result is in agreement with that reported in previous research (Grecu and Krajewski, 2000; Turner *et al.*, 2004; Montanari *et al.*, 2006) such that the moving average window acts like a low-pass filter, and the perishable, high-frequency, and small-scale information is averaged out.

As shown in Table 2, the best performances for all four models were obtained for the slow moving stationary storm event 4, and the worst performances were obtained for the

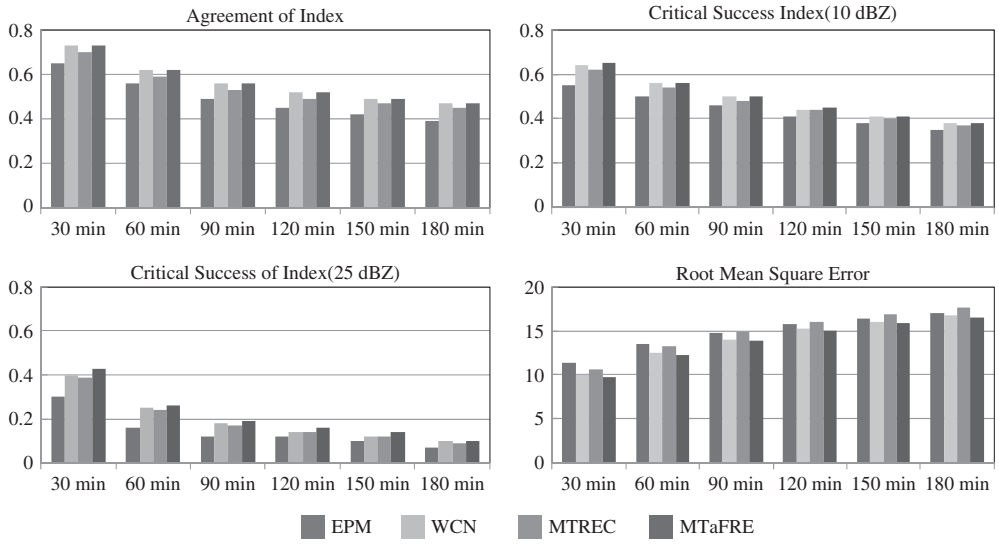

Figure 7. Average forecast performance indices over 1 month evaluation with different lead times.

small and rapidly moving storm, event 5. These results agree with those in previous studies, such that large coherent systems are significantly more persistent than small isolated storms (Germann and Zawadzki, 2002).

5.2. Forecast performances as a function of lead time

Figures 4–6 and Tables 3 and 4 show all the performance indices of obtained forecasts for lead times from 30 to 180 min. In general, the forecast accuracy decreased with increasing lead time for all models. Although the correlation co-efficient was relatively low for lead times up to 180 min, the index of agreement is still satisfactory in the forecast range. For different lead times, the values of the index of agreement varied from 0.28 to 0.77 for the WCN model, from 0.27 to 0.75 for the MTREC, and from 0.28 to 0.78 for the MTaFRE model (see Table 4).

A comparison of Figures 4 and 5 reveals that increasing assessment thresholds of radar reflectivity intensity lead to a decrease in CSI due to lower advection areas based on the intensity–size relationship (Germann and Zawadzki, 2002).

To obtain statistically meaningful inter-comparison results, the verification proceeded over the period from 1 to 31 August 2009. In summary, average performance indices over the period are given in Figure 7. The indices reveal that the EPM performs worse than the three LPM models, the MTREC model performs slightly worse than the WCN, and the MTaFRE model is the most comparable to the WCN one.

6. Conclusions

This paper presents the results of an inter-comparison of four nowcasting models based on radar mosaic patterns from the Jianghuai River Basin, China. The forecast performances were evaluated as a function of lead times of 30 to 180 min at a spatial resolution of $0.01^\circ \times 0.01^\circ$, with emphasis on an assessment of the nowcasting schemes used in the Laboratory of Severe Weather (LaSW) of the Chinese Academy of Meteorological Science (CAMS).

At the individual event level, the inter-comparison showed that no single nowcasting model outperformed others across all categories for every event. For example, the Eulerian Persistence Model (EPM) performed worse than the other three Lagrangian persistent models (LPM) but was competitive with the Watershed-Clustering Nowcasting (WCN) after the 60 min lead time for the slow moving stationary storm event 4, in which the storm almost kept stationary during the period of 90 min. (Figure 8). The Multi-scale Tracking and Forecasting Radar Echoes (MTaFRE) model performed the best for event 3, but was worse than WCN and EPM for event 4 after the 60 min lead time. At a statistics level based on 1 month of radar data, LPM models generally outperformed the EPM. Among LPM models, the Multi-scale Tracking Radar Echoes by Cross-correlation (MTREC) model performed slightly worse than WCN, and MTaFRE was the most comparable to WCN. More important to the objective of this study, the results confirm clearly that the MTaFRE improved upon its predecessor MTREC in forecast accuracy at a range of forecast lead time effectively by using a different moving mean window.

MTaFRE as an extrapolation technique still presents challenges in forecasting the evolution of storm intensity. Other extrapolation methods such as artificial neural networks or autoregressive models do not always show significant improvement of the forecast to model the dynamic Lagrangian evolution of a storm (Grecu and Krajewski, 2000; Montanari *et al.*, 2006). Their common problem lies in the fact that the forecasting skill decreases rapidly with increasing lead time. Alternatively, a mesoscale numerical weather prediction (NWP) model, which assimilates a variety of high-resolution observations, has been developed rapidly in recent years, and the forecast accuracy is relatively stable with increasing lead time. Therefore, these recent developments suggest that a viable path for improving the 0–6 h quantitative precipitation forecast is through the blending of extrapolation and NWP methods, likely with manipulations of the subjective expert inputs to different extents (Wilson and Xu, 2006, Wong *et al.*, 2009). This topic will be explored in future research.

Acknowledgements

This study was supported by the Special Fund for Basic Research and Operation of the Chinese Academy of Meteorological Science (Grant No. 2011Y004), and by the National

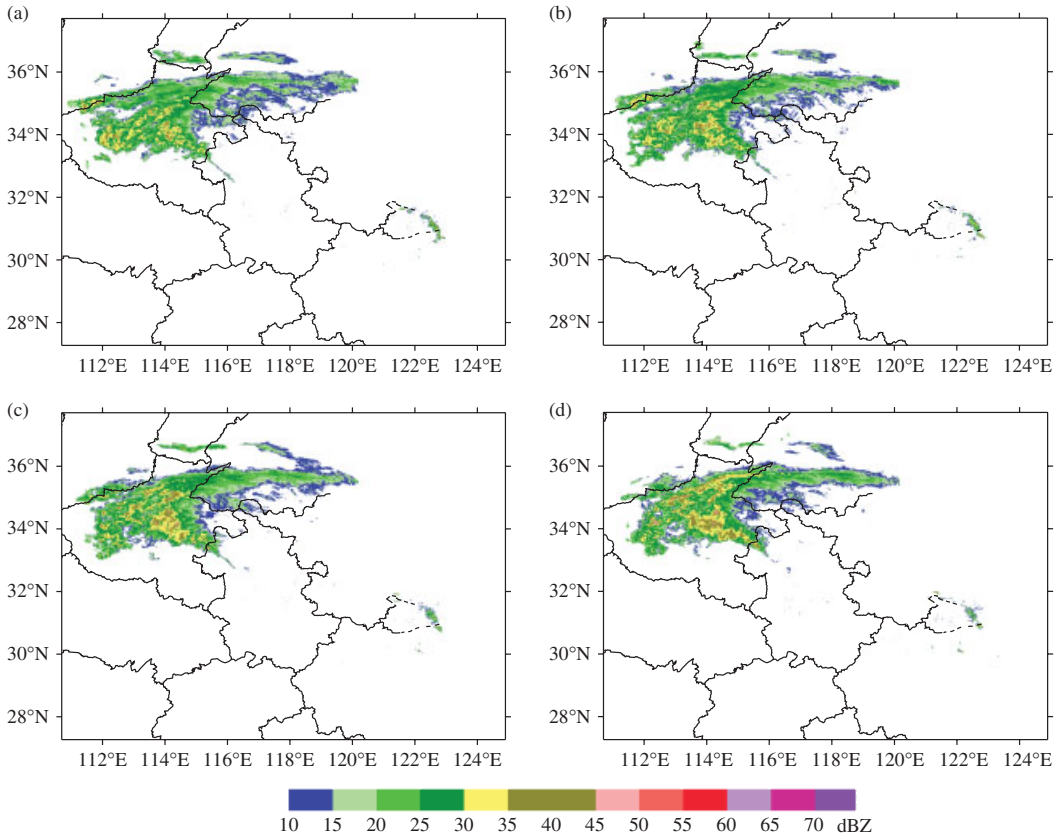

Figure 8. Mosaic images of stationary storm event 4. 0300 UTC (a), 0330 UTC (b), 0400 UTC (c), 0430 UTC (d) on 24 September 2009, respectively.

Natural Science Foundation of China (Grant No. 40975014). The authors also acknowledge the computational facility provided by the HyDROS lab (http://hydro.ou.edu) at the National Weather Centre Advanced Radar Research Centre (http://arrc.ou.edu).

References

Bellon A, Zawadzki I. 1994. Forecasting of hourly accumulations of precipitation by optimal extrapolation of radar maps. *J. Hydrol.* **157**: 211–233.

Benjamin SG, Devenyi D, Weygandt SS, Brundage KJ, Brown JM, Grell GA, Kim D, Schwartz BE, Smirnova TG, Smith TL, Manikin GS. 2004. An hourly assimilation-forecast cycle: the RUC. *Mon. Weather Rev.* **132**: 495–518.

Caya A, Sun J, Snyder C. 2005. A comparison between 4D Var and the ensemble Kalman filter technique for radar data assimilation. *Mon. Weather Rev.* **133**: 3081–3093.

Dixon M, Wiener G. 1993. TITAN: thunderstorm identification, tracking, analysis and nowcasting – a radar-based methodology. *J. Atmos. Oceanic Technol.* **10**: 785–797.

Ganguly AR, Bras RL. 2003. Distributed quantitative precipitation forecasting using information from radar and numerical weather prediction models. *J. Hydrometeorol.* **4**(6): 1168–1180.

Germann U, Zawadzki I. 2002. Scale-dependence of the predictability of precipitation from continental radar images. Part I: description of the methodology. *Mon. Weather Rev.* **130**(12): 2859–2873.

Germann U, Zawadzki I. 2004. Scale-dependence of the predictability of precipitation from continental radar images. Part II: probability forecasts. *J. Appl. Meteorol.* **43**(1): 74–89.

Germann U, Zawadzki I, Turner B. 2006. Predictability of precipitation from continental radar images. Part IV: limits to prediction. *J. Atmos. Sci.* **63**: 2092–2018.

Golding BW. 1998. Nimrod: a system for generating automated very short range forecasts. *Meteorol. Appl.* **5**: 1–16.

Grecu M, Krajewski WF. 2000. A large-sample investigation of statistical procedures for radar-based short-term quantitative precipitation forecasting. *J. Hydrol.* **239**: 69–84.

Hong Y, Hsu K, Sorooshian S, Gao X. 2004. Precipitation estimation from remotely sensed imagery using an Artificial Neural Network cloud classification system. *J. Appl. Meteorol.* **43**: 1834–1853.

Houze RA, Schmid W, Fovell RG, Schiesser HH. 1993. Hailstorms in Switzerland: left movers, right movers, and false hooks. *Mon. Weather Rev.* **121**: 3345–3370.

Johnson JT, MacKeen PL, Witt A, Mitchell ED, Stumpf GJ, Eilts MD, Thomas KW. 1998. The storm cell identification and tracking algorithm: an enhanced WSR-88D algorithm. *Weather Forecast.* **13**: 263–276.

Lakshmanan V, Rabin R, DeBrunner V. 2003. Multiscale storm identification and forecast. *J. Atmos. Res.* **67**: 367–380.

Lakshmanan V, Smith T, Stumpf GJ, Hondl K. 2007a. The warning decision support system – integrated information. *Weather Forecast.* **22**(3): 596–612.

Lakshmanan V, Fritz A, Smith T, Hondl K, Stumpf GJ. 2007b. An automated technique to quality control radar reflectivity data. *J. Appl. Meteorol.* **46**: 288–305.

Lakshmanan V, Hondl K, Rabin R. 2009. An efficient, general-purpose technique for identifying storm cells in geospatial images. *J. Atmos. Oceanic Technol.* **26**: 523–537.

Lakshmanan V, Smith T. 2009. Data mining storm attributes from spatial grids. *J. Atmos. Oceanic Technol.* **26**: 2353–2365.

Lakshmanan V, Smith T. 2010. An objective method of evaluating and devising storm tracking algorithms. *Weather Forecast.* **25**(2): 721–729.

Lakshmanan V, Zhang J, Howard K. 2010. A technique to censor biological echoes in radar reflectivity data. *J. Appl. Meteorol.* **49**: 435–462.

Legates DR, McCabe GJ. 1999. Evaluating the use of goodnessof-fit measures in hydrologic and hydroclimatic model validation. *Water Resour. Res.* **35**(1): 233–241.

Li L, Schmid W, Joss J. 1995. Nowcasting of motion and growth of precipitation with radar over a complex orography. *J. Appl. Meteorol.* **34**: 1286–1300.

Liang QQ, Feng YR, Deng WJ, Hu S, Huang YY, Zeng Q, Chen ZT. 2009. A composite approach of radar echo extrapolation based on TREC vectors in combination with model-predicted winds. *Adv. Atmos. Sci.* **27**(5): 1119–1130.

Macpherson B. 2001. Operational experience with assimilation of rainfall data in the Met Office Mesoscale model. *Meteorol. Atmos. Phys.* **76**: 3–8.

Montanari L, Montanari A, Toth E. 2006. A comparison and uncertainty assessment of system analysis techniques for short-term quantitative precipitation nowcasting based on radar images. *J. Geophys. Res.* **111**: D14111, DOI: doi.org/10.1029/2005JD006729.

Pradeep VM, Germann U, Panziera L, Hering A. 2012. Can Lagrangian extrapolation of radar fields be used for precipitation nowcasting over complex alpine orography? *Weather Forecast.* **27**: 28–49.

Qi YC, Zhang J, Zhang PF. 2013. A real-time automated convective and stratiform precipitation segregation algorithm in native radar coordinates. *Q. J. R. Meteorol. Soc.* **139**: 2233–2240, DOI: 10.1002/qj.2095.

Reich S. 2007. An explicit and conservative remapping strategy for semi-Lagrangian advection. *Atmos. Sci. Lett.* **8**: 58–63.

Rinehart R, Garvey E. 1978. Three-dimensional storm motion detection by conventional weather radar. *Nature* **273**: 287–289.

Seed AW. 2003. A dynamic and spatial scaling approach to advection forecasting. *J. Appl. Meteorol.* **42**: 381–388.

Sokol Z. 2007. Utilization of radar reflectivity for a very short range precipitation forecast. *Czech Meteorol. Bull.* **60**: 136–146.

Sokol Z, Pesice P. 2012. Nowcasting of precipitation-advection statistical 17 forecast model (SAM) for the Czech Republic. *J. Atmos. Res.* **103**: 70–79.

Tong M, Xue M. 2005. Ensemble Kalman filter assimilation of Doppler radar data with a compressible nonhydrostatic model: OSS experiments. *Mon. Weather Rev.* **133**: 1789–1807.

Tsonis AA, Austin GL. 1981. An evaluation of extrapolation techniques for the short-term prediction of rain amounts. *Atmos.-Ocean.* **19**: 54–65.

Turner B, Zawadzki I, Germann U. 2004. Predictability of precipitation from continental radar images. Part III: operational nowcasting implementation (MAPLE). *J. Appl. Meteorol.* **43**: 231–248.

Tuttle JD, Foote GB. 1990. Determination of the boundary layer airflow from a single doppler radar. *J. Atmos. Oceanic Technol.* **7**: 218–232.

Tuttle J, Gall R. 1999. A single-radar technique for estimating the winds in tropical cyclones. *Bull. Am. Meteorol. Soc.* **80**: 653–668.

Vila DA, Machado LA, Laurent H, Velasco I. 2008. Forecast and Tracking the Evolution of Cloud Clusters (ForTraCC) using satellite infrared imagery: methodology and validation. *Weather Forecast.* **23**: 233–245.

Wang GL, Liu LP, Ding YY. 2012. Improvement of radar quantitative precipitation estimation based on real-time adjustments to Z-R relationships and inverse distance weighting correction schemes. *Adv. Atmos. Sci.* **29**(3): 575–584.

Wang GL, Wong WK, Liu LP, Wang HY. 2013. Application of multi-scale tracking radar echoes scheme in quantitative precipitation nowcasting. *Adv. Atmos. Sci.* **30**(2): 448–460.

Wang HY, Liu LP, Wang GL, Zhang W, Zhang ZQ, Chen XL. 2009. Development and application of the doppler weather radar 3-D digital mosaic system. *J. Appl. Meteorol. Sci.* **20**(2): 241–224 (in Chinese).

Weygandt SS, Shapiro A, Droegemeier KK. 2002. Retrieval of model initial fields from single-Doppler observations of a supercell thunderstorm. Part I: single-Doppler velocity retrieval. *Mon. Weather Rev.* **130**: 433–453.

Wilson JW, Brandes EA. 1979. Radar measurement of rainfall – a summary. *Bull. Am. Meteorol. Soc.* **60**(9): 1048–1058.

Wilson J, Xu M. 2006. Experiments in blending radar echo extrapolation and NWP for nowcasting convective storms. *Proceedings of the Fourth European Conference on Radar in Meteorology and Hydrology*. Barcelona, Spain; 519–522.

Wong WK, Yeung HY, Wang YC, Chen M. 2009. Towards the blending of NWP with nowcast-operation experience in B08FDP. *WMO Symposium on Nowcasting*. 30 August–4 September 2009. Whistler, B.C. Canada.

Xiao YJ, Liu LP. 2006. Study of methods for interpolating data from weather radar network to 3-D grid and mosaics. *Acta Meteorol. Sin.* **64**(5): 647–656(in Chinese).

Xu XY, Howard K, Zhang J. 2008. An automated radar technique for the identification of tropical precipitation. *J. Hydrol.* **9**: 885–902.

Zahraei A, Hsu K, Sorooshian S, Gourley JJ, Hong Y, Lakshmanan V, Bellerby T. 2012. Quantitative precipitation nowcasting: a Lagrangian pixel-based approach. *J. Atmos. Res.* **118**: 418–434.

Zahraei A, Hsu K, Sorooshian S, Gourley JJ, Hong Y, Behrangi A. 2013. Short-term quantitative precipitation forecasting using an object-based approach. *J. Hydrol.* **483**: 1–15.

Zawadzki I. 1984. Factors affecting the precision of radar measurements of rain. Preprints. *22nd International Conference on Radar Meteorology*, Zurich, Switzerland, Amer. Meteor. Soc. 251–256.

Zhang J, Howard K, Xia W, Langston C, Wang S, Qin YC. 2004. Three-dimensional high-resolution national radar mosaic. Preprints (CD-ROM). *The 11th Conference on Aviation, Range, and Aerospace Meteorology*, Amer. Meteor. Soc. 4–8 October 2004, Hyannis, MA.

Zhang YP, Chen MH, Xia WM, Cui ZH, Yang HP. 2006. Estimation of weather radar echo motion field and its application to precipitation nowcasting. *Acta Meteorol. Sin.* **64**(5): 631–646 (in Chinese).

